Version of Record: https://www.sciencedirect.com/science/article/pii/S0278434321000790
Manuscript_49a423cba9e9e0faf2e6499a43347fb4

Boat wake effects on sediment transport in intertidal waterways

Ilgar Safak[a*], Christine Angelini[b,c], Alex Sheremet[b]

a. Department of Civil Engineering, Faculty of Engineering and Natural Sciences, Istanbul Bilgi University, Eski Silahtaraga Elektrik Santrali, 34060 Eyupsultan, Istanbul, TURKEY

b. Civil and Coastal Engineering Department, Engineering School of Sustainable Infrastructure & Environment, University of Florida, 365 Weil Hall, P.O. Box 116590, Gainesville, FL 32611, USA

c. Department of Environmental Engineering Sciences, Engineering School of Sustainable Infrastructure & Environment, University of Florida, 365 Weil Hall, P.O. Box 116590, Gainesville, FL 32611, USA

Abstract

Boat traffic and resulting wakes are among the major human-mediated stressors on coastal ecosystems. Modulation of sediment transport by wakes and tides in an intertidal waterway with boat traffic is studied here. The hypothesis that boat wakes cause significant increases in sediment transport in intertidal settings is tested. Field observations of tides, currents, boat wakes and turbidity were collected on a transect within the Atlantic Intracoastal Waterway in Northeast Florida, USA. Hydrodynamic and sediment processes were evaluated by analyzing this field data set. A daily average of 60 wake events of varying energies were identified in the observations using time-frequency analysis methods. Due to differences in sediment suspension in response to each wake and unpredictable evolution of the bed state, decomposition of the effects of each individual wake on sediment is not possible. Therefore, the sediment dynamics during the periods of boat activity were compared in their entirety with the sediment dynamics during the periods of boat inactivity. Throughout the experiment, all periods of boat activity had consistently greater suspended sediment concentration near the bed compared to their preceding and succeeding periods of boat inactivity. In the first eight days of

*Corresponding author. E-mail: ilgar.safak@bilgi.edu.tr

the experiment where tidal forcing was relatively similar between boat activity and inactivity periods, sediment transport rates were estimated as 0.048 m^3/m/hr and 0.043 m^3/m/hr during boat activity and inactivity, respectively, indicating a 12% increase in sediment transport due to boat traffic. A larger increase in sediment transport rates during boat activity compared to boat inactivity occurred over the last three days of the experiment. Volumes of sediment transported in low-tide, mid-tide and high-tide during boat activity were greater than their low-tide, mid-tide and high-tide counterparts during boat inactivity. Therefore, the results confirm the earlier mentioned hypothesis.

Keywords: boat wakes; waves; sediment transport; sediment flux; tides; erosion; intertidal; coastal ecosystem; Florida; Intracoastal Waterway

1 Introduction

One of the major and growing human-mediated threats on coastal ecosystems is boat traffic that is experiencing a significant growth worldwide (Tournadre, 2014). In intertidal settings, such as estuaries, shallow coastal bays and waterways that experience boat traffic, wakes of these boats create an important hydrodynamic forcing, alongside tides, on coastal ecosystems (e.g., vanStraaten and Kuenen, 1958; Green and Coco, 2007; Wiberg et al., 2015). Boats and their wakes have direct negative impacts on coastal flora and fauna (e.g., Gabel et al., 2017). In addition, they pose threat on shoreline and seafloor stability, light availability and water quality due to the potential of waves to resuspend the sediment at the seafloor and make it available for advection by currents in intertidal areas and shallow bays (e.g., Loosanoff, 1962; Schwimmer, 2001; Price, 2005; Lawson et al., 2007; Mcloughlin et al., 2015). Although recreational boat activity for cruising and fishing can also support coastal economies, boat traffic and resulting waves have been reported to significantly enhance shoreline erosion in sheltered estuaries where waves would have relatively small impact on shoreline in absence of this traffic (e.g., Bilkovic et al., 2019). Therefore, better understanding of the impacts of boat wakes on fate of sediment is necessary to inform robust strategies for improving ecosystem health, shoreline stability and efficient management of dredging, maintenance and navigational needs in intertidal and intracoastal waters.

Investigations of boat wake effects on sediment transport have mostly been qualitative (Osborne and Boak, 1999; Parnell et al., 2007) or focused on the physics of suspension of sediment during individual wake events (Houser, 2011; Malej et al., 2019) and have not taken tidal stages or currents into account (Bauer et al., 2002; Houser, 2011; De Roo and Troch, 2015). Studies on the effects of tides and wakes on sediment processes (e.g., Styles and Hartman, 2019) focused on limited number of wake events in data sets of relatively short periods (~40 hours) and neither integrated sediment fluxes throughout the water column nor evaluated the wake impacts on cumulative sediment fluxes within the studied systems. As a result, there is a strong need for research on the effects of boat wakes on sediment processes in intertidal settings and modulation of these processes by tides. It is hypothesized here that boat wakes could have significant effects on sediment transport in intertidal waterways. To test this hypothesis, in this study, field observations of boat wakes, tides and sediment processes were collected in an intertidal setting (Section 2.1) and analyzed (Section 2.2). The results obtained from the observations of tides and currents, boat wakes, and sediment processes are evaluated (Section 3) and then used for discussing the impacts of wakes and tides on sediment transport dynamics in intertidal areas (Section 4). The findings are summarized in Section 5.

2 Method

2.1 Field experiment

The field observations were collected at the Tolomato River channel in Guana Tolomato Matanzas National Estuarine Research Reserve (GTMNERR, hereafter GTM for brevity) within St. Johns County in Northeast Florida, USA (Figure 1a) between 23 May and 3 June in 2019. The field site (29.986391° Latitude North, 81.327358° Longitude West) is located 9 km north of St. Augustine Inlet and 47 km south of St. Johns Inlet, where the Guana River connects to the Tolomato River (Figure 1a). GTM is within the Atlantic Intracoastal Waterway and experiences year-round traffic of navigational and recreational boats (FLHSMV, 2013; Montes et al., 2016; FDEP, 2018). Based on the aerial photographs of 65-km-long intracoastal channel margin along GTM, it was found that 70 hectares of shoreline habitat (bars, marsh) eroded between 1970 and 2002 (Price, 2005). This can be roughly converted into a shoreline erosion rate of 0.35 m/yr on average along the analyzed section. This shoreline erosion rate is in the same order of magnitude as those that were recently measured along the Intracoastal Waterway, at about 35 km south of our study site (Silliman et al., 2019). The related analysis also revealed that exposure to boat wakes are likely the primary cause of this erosion. For further details about the GTM and its boat traffic, wake climate and shoreline habitat erosion rates, the reader is referred to Safak et al. (2020a) and Safak et al. (2020b).

The coastline at the location of the experiment is oriented ~15^o counterclockwise from the North-South orientation (Figure 1a). Based on the sediment samples collected, surficial sediment at the study site is characterized as fine sand with a median diameter of D_{50}=200 μm (Herbert et al., 2018). The Tolomato River channel is about 400 m wide at the experiment location (Figure 1); a sand bar, which emerges in low-tide, is located about 30 m offshore of the coastline. The hydrodynamic measurements were collected at two locations offshore of the sand bar (Figure 1b). An acoustic velocimeter, Nortek Vector with 6 MHz frequency of acoustic signal transmission, was located at each of the two points that were on a 13-m-long cross-channel transect. Point A, located about 57 m from the shoreline, had a mean depth of 1.09 m averaged over the experiment duration (Figure 1b). Point B, the shallow point that was located 13 m onshore of A, had an average depth of 0.65 m and was dry during low-tide (Figure 1b). The cross-channel slope of the seafloor between the two measurement points was about 1/30. The velocimeters made point measurements of pressure, flow velocity and acoustic backscatter continuously at 8 Hz sampling frequency. Quality control on the data sets was conducted. Data with along-beam signal correlations less than 90% were marked as low-quality and removed from the analysis (Nortek, 2018). Suspended sediment concentration was estimated using the calibrated acoustic backscatter (e.g., Ozturk and Work, 2016). The sampling volumes of the velocimeters were at 0.17 meters above bed (mab). Winds were analyzed by using the meteorological data collected by the GTM at 29.6578° Latitude North, 81.2328° Longitude West, i.e., 39 km South of the experiment site (NERRS, 2019).

2.2 Data analysis

2.2.1 Hydrodynamic and sediment processes

Depth-integrated horizontal flux of sediment mass per unit width is obtained as

$$q = \int_{-h}^{0} u(z)\, c(z)\, dz\,, \tag{1}$$

based on the measurements of currents (u) and suspended sediment concentration (c), and their estimated vertical structures. h is the water depth, z is the vertical coordinate which is equal to zero at the water surface and -h at the bed. The vertical structure of horizontal currents, i.e., $u(z)$, is assumed to be logarithmic (Nielsen, 1992):

$$u(z) = \frac{u_*}{\kappa} \ln\left(\frac{z}{z_o}\right)\,, \tag{2}$$

where u_* is the bottom friction velocity and κ=0.41 is the von Karman's constant. Furthermore, z_o is the zero-intercept level where the horizontal velocity is assumed to be zero and is related to the hydraulic roughness length (k_s) as $z_o = k_s/30$. Hydraulic roughness length is assumed to be related to a flat bed. Accordingly, $k_s = 2D_{50}$ where D_{50} is the median diameter of sediment (Nielsen, 1992) and z_o=0.000013 m. The shear stress at the bed is estimated as $\tau_b = \rho u_*^2$ where ρ is the density of water.

The vertical structure of suspended sediment concentration ($c(z)$) is obtained using the Rouse profile which is based on a balance between upward diffusion and downward settling of sediment (Rouse, 1937, 1961; Mofjeld and Lavelle, 1988)

$$c(z) = \frac{E}{w_s}\left[\frac{z}{z_o}\,\frac{(h-z_o)}{(h-z)}\right]^{-w_s/\kappa u_*}\,, \tag{3}$$

where E is the erosion rate and w_s is the sediment settling velocity taken as 0.03 cm/s for fine sand of D_{50}=200 μm. For each 10 minute measurement interval, q, u_* and E are obtained based on the Equations 1, 2 and 3 using the near-bed observations of mean currents and suspended sediment concentration; then the vertical structures throughout the water column are constructed. This procedure averages over the waves as well.

As demonstrated later in Section 3, sediment suspension and settling vary from one wake event to another. This is due to both the variations in physical forcing (e.g., wake energy, tidal phase) and the unremitting and unpredictable evolution of the state of the sea bed (whether it is consolidated or soft). Besides these variations, there are uncertainties associated with the background levels of SSC and bed state in the absence of wakes which together make filtering the effects of each individual wake on boundary layer processes, bed shear stresses, and, eventually, SSC levels infeasible. Therefore, in this study, the sediment transport during the periods of boat activity and the resulting wake energies is compared in its entirety with the sediment transport during the periods of boat inactivity. While the beginning and ending times of boat activity and boat inactivity periods show small variations from one day to another, the periods of boat activity and inactivity correspond to virtually equal 12-hr-long intervals on average from 7:30 AM to 7:30 PM, and from 7:30 PM to 7:30 AM, respectively. Modulation of sediment processes by tides is investigated by comparing the sediment fluxes at varying water levels (low-tide, mid-tide, high-tide) and at parts of the experiment with different tidal forcing (relatively small and relatively high tidal fluctuations and resulting currents and bed stresses). The deployment period covered both neap and spring tides.

2.2.2 Boat wakes

Due to their transient nature and relatively short timescales (seconds - minutes), boat wakes appear in data as *'chirp'* signals. Identification of boat wakes in field observations requires the use of advanced methods of time-frequency analysis. First, the effects of tides in the pressure signal measured near the bed are filtered out. Applying a windowed Fourier transform and wavelet transform to the de-tided data gives a spectrogram, in which the wakes are identified by the monotonically increasing peak frequency where the energy is highest. To estimate the height of each wake, pressure variation at the water surface is obtained from the de-tided pressure data measured near the bed, by taking into account the vertical structure of pressure throughout the water column based on the linear wave theory. Once the sea surface elevation is obtained, the height of the highest wave and the corresponding period are recorded for each wake. For details of the identification of boat wakes in the field observations and the related time-frequency data analysis methods, the reader is referred to Sheremet et al. (2013).

3 Results

3.1 Tides and currents

The general conditions throughout the field experiment are summarized in Figure 2. Semi-diurnal tides dominated the water depth variations (Figure 2a) at both Station A (mean depth of 1.09 m during the experiment) and Station B (mean depth of 0.65 m). The average tidal range was about 1.2 m (Figure 2a). Station B was dry (i.e., the sensor was emerged during low tide) for 31% of the total duration of the experiment (Figure 2a), while Station A was submerged for the entire duration of the experiment. Current flow was along the North-South axis (Figure 3a). Wind climate was almost entirely northward in the North-South orientation during the experiment: north-northwestward winds between 3 m/s and 5 m/s, and north-northeastward winds between 1 m/s and 3 m/s (Figures 2b and 3b). Similar to the water depth variations, currents were also dominated by the tidal forcing (Figure 2c). As might be expected, bed shear stresses very closely followed current speeds (Figure 2d). The other feature apparent in the currents is the asymmetry such that northward flows and associated shear stresses at the bed were stronger than southward flows and associated bed stresses (Figures 2c-d and 3a). This difference is attributed to the wind climate (Figures 2b and 3b). The near-bed flows (0.17 mab) at Station A were about 35% stronger than those at Station B (Figures 2c and 3c). The concentrations of suspended sediment at 0.17 meters above bed at Station B were twice as high as those at Station A (Figures 2e and 3d).

3.2 Wakes

Spectrograms obtained by applying a windowed Fourier transform and wavelet transform to the de-tided data on two five-minute-long time segments – one that did not contain any boat wakes and one with boat wakes– are demonstrated in Figure 4. Within the time segment with boat wakes, monotonically increasing peak frequency where the energy is highest is evident and help identify the wakes in the data.

Based on the spectrogram analysis, a total of 661 wake events were detected during the experiment. Resulting waves most commonly had heights of ~0.1 m (Figure 5a) and periods of ~1.7 s (Figure 5b). In the most energetic events, wake heights and periods reached 0.5 m and 5 s, respectively (Figure 5). Contribution of winds to these observed waves and the wave climate of the study site is negligible considering the limited fetch and wind conditions during the experiment (Safak et al., 2020a).

3.3 Sediment processes

As an example, Figure 6 shows variations of water levels and suspended sediment concentration (SSC) during the day (boat activity and resulting wakes) and night (boat inactivity; no wakes) are shown for one day. The fluctuations in water levels and increases in SSC due to the boat traffic during the day and resulting wakes are evident. To demonstrate the effect of individual wakes, a 30-min-long time series of water levels, flow velocity and SSC are shown in Figure 7. As previously explained in Section 2.2.1, different wakes are seen to cause sediment suspensions of varying concentrations (enhanced by an order of magnitude in some wake events) due to varying wave-induced orbital velocities and different behaviors of settling that occurs after the wake passes by (Figure 7).

Based on the field observations (Section 2.1) and the analysis approaches detailed in Section 2.2.1, vertical structures of currents, vertical structures of SSC, and finally the sediment transport at the two points on the cross-channel transect are obtained (Figure 8). The higher SSC values throughout the entire water column during the periods of boat activity compared to those during boat inactivity are evident (Figure 8a and b). Between 23 May and 30 May, the peaks of horizontal sediment transport per unit width were 0.1-0.15 m^3/m/hr at both depths (Figure 8c); the period of 31 May - 2 June had evidently greater peaks that reached 0.4 m^3/m/hr (Figure 8c). The horizontal sediment fluxes estimated at Station A were consistently greater than those at B.

Variations of concentration of suspended sediment and volume of transported sediment integrated separately over the periods of boat activity and boat inactivity are summarized in Figure 9. The daily average of number of wake events is about 60. During weekdays, an average of about 45 wake events were observed. Saturday, Sunday and Memorial Day Monday had greater number of wake events reaching 80 due to holiday traffic (Figure 9a). All boat activity periods are associated with greater SSC and volume of sediment transported, compared to their preceding periods of boat inactivity (Figure 9b and c). Throughout the experiment, average SSC during the periods of boat activity is greater than the one during the periods of boat inactivity (Figure 9b). Total volume of sediment transported per unit width (Figure 9c) throughout the experiment was estimated as 13.72 m^3/m (Table 1), 60% of which was estimated to occur during boat activity (8.28 m^3/m) and 40% during boat inactivity (5.44 m^3/m).

4 Discussion

4.1 Modulation of sediment transport by tides and wakes

Based on the results presented in Section 3, the impacts of tidal variations and boat wake activity in modulating sediment transport processes are investigated in detail here. There are two major differences in sediment transport dynamics between the last three-day-period of spring tides (31 May - 2 June; annotated with *LT* in Figure 2) and the first eight-day-period of the experiment (23 May - 30 May). First, the *LT* period is characterized by greater sediment flux peaks over the tidal cycles (Figure 8c). Second, within *LT*, the peak fluxes and integrated fluxes within the boat activity periods are evidently greater than those within the boat inactivity periods, in contrast to the comparable peaks and integrations over the periods of boat activity and inactivity during the previous part of the experiment (Figures 8c and 9c). These two features are attributed to the difference in the dynamics of tides and currents between these two intervals: First, the *LT* period had larger tidal fluctuations (1.5 m on average) compared to the previous part of the experiment (1.1 m on average; Figure 2a). These amplitudes of tidal fluctuations during these two periods are consistent with the data reported by the closest tidal gauge of the National Oceanic and Atmospheric Administration (NOAA; Station ID: 8720218) located near St. Johns Inlet. These larger tidal fluctuations during the *LT* period triggered stronger currents of 0.35 - 0.40 m/s (versus 0.27 - 0.29 m/s; Figure 2c) and higher bed stresses (>0.2 Pa reaching 0.32 Pa; versus ~0.15 Pa; Figure 2d). Second, there is a tidal-phase-induced asymmetry in bed stresses between the periods of boat activity and inactivity during *LT*: the stresses are much greater during the boat activity periods in contrast to the relatively similar bed stresses during boat activity and inactivity periods within the previous part of the experiment (Figure 2d). Note also that there is no comparable peak in stress in the boat inactivity period of 1 June but there are two peaks in the boat activity period of 2 June.

As a result, the sediment transport processes are evaluated separately for these two parts of the experiment. Total sediment volumes per unit width are obtained by integrating the depth-averaged sediment fluxes separately over the boat activity and inactivity periods. These volumes are standardized by taking into account the durations of these periods; and the sediment transport rates are obtained. For *LT*, the average sediment transport rate for the boat activity periods (0.085 m^3/m/hr) is about twice as much as the one for the boat inactivity periods (0.040 m^3/m/hr; Table 1). For the first eight days, when there was no such asymmetry between the periods of boat activity and inactivity in terms of currents, sediment transport was still more abundant during the boat activity periods (0.048 m^3/m/hr vs 0.043 m^3/m/hr; Table 1). In spite of the smaller difference compared to the *LT* period, this 12% enhancement in sediment transport rates during the boat activity period shows that boat activity and resulting wakes are significant factors controlling sediment dynamics in intertidal waterways.

Modulation of the sediment transport by water levels is shown in Figure 10 separately for the first eight-day-period and the last three-day-period of the experiment. During both the boat activity and inactivity periods in these two sections of the experiment, volume of transported sediment shows an overall increasing trend with increasing water levels (Figure 10). Average volumes of sediment transported at low-tide, mid-tide and high-tide conditions during the periods of boat activity are estimated to be greater than their low-tide, mid-tide and high-tide counterparts during the periods of boat inactivity (Figure 10). Although the difference appears to be more evident in the second part of the experiment due to the current-related effects detailed above (Figure 10b), the sediment transport during boat activity is greater on average than the one during boat inactivity at all water levels in the first part of the experiment as well (Figure 10a).

4.2 Effect of ripples

In settings where wind waves (assumed to be stationary over time scales of hours) are prominent, ripples could form at the bed and affect the hydraulic roughness, bottom friction, and, eventually, the vertical structures of flow and sediment transport. Boat wakes could affect these processes as well, however, how they affect and whether ripples can form and sustain under these wakes are unknown due to the transient nature and much shorter time scales (seconds - minutes) of the wakes. Despite these uncertainties and instrumentation-related limitations on observing these processes (i.e., measurements at a single point in the vertical throughout the water column), possible effect of ripples on sediment transport rates here is investigated. Ripple height (η) and ripple length (λ) are estimated by using the following relationships (Styles and Glenn, 2002)

$$\frac{\eta}{A_b} = \begin{cases} 0.30X^{-0.39}, & X \leq 2 \\ 0.45X^{-0.99}, & X \geq 2 \end{cases} , \tag{4}$$

$$\frac{\lambda}{A_b} = \begin{cases} 1.96X^{-0.28}, & X \leq 2 \\ 2.71X^{-0.75}, & X \geq 2 \end{cases} , \tag{5}$$

where A_b is the bottom wave excursion amplitude, and X is the ratio of the nondimensional mobility number (θ_m) to the nondimensional sediment parameter (S_*)

$$A_b = \frac{u_b T}{2\pi} \ , \ u_b = \frac{H\pi}{sinh(kh)T} \ , \tag{6}$$

$$X = \frac{\theta_m}{S_*} \ , \ \theta_m = \frac{u_b^2}{(s-1)gD} \ , \ S_* = \frac{D}{4\nu}\sqrt{(s-1)gD} \ , \tag{7}$$

where u_b is the bottom wave orbital velocity, T is wave period, H is wave height, k is wave number, s is the specific gravity of sediment (2.65), g is the gravitational acceleration, D is the sediment diameter taken equal to the median diameter of 200 μm here, and ν is the kinematic viscosity of water. For each wake event detected, the ripple geometry was estimated using this methodology. Then, ripple-induced hydraulic roughness (k_{s-r}) was estimated using the following relationship based on the observations of ripple formation under oscillatory flow (Nielsen, 1992)

$$k_{s-r} = 8\frac{\eta^2}{\lambda} \ . \tag{8}$$

The corresponding z_{o-r}, equal to $k_{s-r}/30$, is added to the z_o, which is related to a flat bed, in Eqs. 2 and 3 to estimate the modified flow, sediment concentration, and sediment transport rates. Wave and flow conditions in more than two-thirds of the detected wake events here resulted in an estimated ripple height of η=0.6-0.8 cm, a ripple length of λ=4-6 cm, and a z_{o-r}~0.0003 m, the last of which is an order of magnitude greater than the one for a flat bed. The sediment transport rates obtained by using this z_{o-r} that takes the boat-wake-induced ripple effects into account over the boat activity periods are calculated to be 6% greater than those obtained by assuming a flat bed over those boat activity periods. This indicates the possibility that estimates of sediment transport rates during boat activity could be subject to an even further increase in case of wake-induced rippled formation, however, it has to be noted that whether and how boat wakes form ripples can not be fully determined due to the aforementioned uncertainties. Evaluation of this possible further enhancement in sediment transport and the overall impact of boat wakes on sediment processes can be improved by collection of high-resolution data on bottom boundary layer and bed state.

5 Conclusions

In this study, the modulation of sediment transport by boat wakes, tides and currents in an intertidal waterway setting with boat traffic was investigated by analyzing field observations. Although being transient and associated with relatively short time scales of minutes, waves that are generated in the wakes of vessels were observed here to resuspend sediment and enhance the sediment concentration by an order of magnitude in some wake events. As a result of an analysis that compares the periods of boat activity/inactivity and takes into account the effects of varying water levels and currents, boat traffic and resulting wakes were shown to cause a significant increase in sediment transport rate in intertidal waterways, even in fetch-limited conditions. Within the first three-quarters of the experiment when the periods of boat activity and inactivity experienced relatively similar tidal forcing, rates of sediment transport per unit cross-channel width were estimated as 0.048 m^3/m/hr and 0.043 m^3/m/hr during boat activity and inactivity, respectively. This indicates a 12% increase in sediment transport due to boat traffic. In the last quarter of the experiment which was modulated by both tides and wakes, twice as much sediment transport rate was estimated for the period of boat activity compared to the one for the period of boat inactivity. Wake-induced increase in sediment transport was detected at all tidal levels. To the best of the authors' knowledge, this study has been the most comprehensive evaluation, so far, of boat wakes on sediment processes in intertidal areas. A large-scale implication of our results is that boat activity, which can contribute to coastal economies, is also a major anthropogenic impact on sheltered estuaries and intertidal waterways due to its influence on hydrodynamics and resulting potential to erode sediment, increase turbidity, decrease water quality. Another large-scale implication of the results here is that reducing the anthropogenic impact on geomorphic evolution and mitigating shoreline erosion in these estuaries and intertidal areas, and management of the stability and functionality of coastal wetlands, reef and mudflat habitats require regulations on boat traffic. It needs to be noted that the observed contribution of boat traffic and resulting wakes in sediment transport is affected by seasonality in traffic and the time of the year the observations were collected (spring season); therefore, there will be periods (i.e., summer season) when the effect of wakes will be even greater than the observed effect here.

One major remaining challenge in understanding the effects of boat traffic on sediment transport in field conditions is that filtering the individual effects of each boat wake on bottom boundary layer processes and sediment transport is not possible. This is because the sea bed state is continuously evolving due to a plethora of processes; i.e., the sediment resuspension potential of a wake is different when it propagates over a bed (i) that is consolidated after periods of relatively low energy, or (ii) which has been softened due to recent high energy conditions. Accordingly, collecting and analyzing observations on bed state simultaneously with data on wake effects on bottom boundary layer (e.g., ripples) and sediment processes can be a potential focus on future studies. Another research gap is within the investigation of the wake structure and resulting sediment transport as a function of vessel properties (type, draft, size, speed). Ongoing efforts include the analysis of the co-located video imagery data, collected for this goal, on the vessel traffic during this experiment, in concert with the hydrodynamic observations.

Acknowledgments

This work was sponsored by the National Estuarine Research Reserve System Science Collaborative, which supports collaborative research that addresses coastal management problems important to the reserves. The Science Collaborative is funded by the National Oceanic and Atmospheric Administration and managed by the University of Michigan Water Center (NAI4NOS4190145). We thank Todd Van Natta and Patrick Norby from the University of Florida for their technical support, and Nicole Dix and Scott Eastman for their logistical support and knowledge of the region. We also would like to thank the Editor-in-Chief Dr.Arnoldo Valle-Levinson and the two anonymous reviewers for the time and effort they spent for providing suggestions towards improving the manuscript.

Conflicts of interest

The authors declare no conflicts of interest.

References

Bauer, G., Lorang, M.S., Sherman, D.J., 2002. Estimating boat-wake-induced levee erosion using sediment suspension measurements. J. Waterw. Port Coas. Ocean Eng. 128(4), 152-162.

Bilkovic, D.M., Mitchell, M.M., Davis, J., Herman, J., Andrews, E., King, A., Mason, P., Tahvildari, N., Davis, J., Dixon, R.L., 2019. Defining boat wake impacts on shoreline stability toward management and policy solutions. Ocean Coas. Manag. 182, 104945.

De Roo, S., Troch, P., 2015. Evaluation of the effectiveness of a living shoreline in a confined, non-tidal waterway subject to heavy shipping traffic. Riv. Res. Appl. 31, 1028–1039. DOI: 10.1002/rra.2790

Florida Department of Environmental Protection, 2018. Critically eroded beaches in Florida. Division of Water Resource Management, 89 p. https://floridadep.gov/sites/default/files/CriticallyErodedBeaches.pdf ; https://ca.dep.state.fl.us/mapdirect/?focus=beaches

Florida Highway Safety and Motor Vehicles, 2012. Vessel owners: Statistics 2011. Florida Department of Highway Safety and Motor Vehicles. http://www.flhsmv.gov/dmv/vslfacts.html.

Gabel, F., Lorenz, S., Stoll, S., 2017. Effects of ship-induced waves on aquatic ecosystems. Sci. Total Environ. 601-602, 926–939.

Green, M.O., Coco, G., 2007. Sediment transport on an estuarine intertidal flat: measurements and conceptual model of waves, rainfall and exchanges with a tidal creek. Estuar. Coas. Shelf Sci. 72(4), 553–569.

Herbert, D., Astrom, E., Bersoza, A.C., Batzer, A., McGovern, P., Angelini, C., Wasman, S., Dix, N., Sheremet, A., 2018. Mitigating erosional effects induced by boat wakes with living shorelines. Sustainability 10 (2), doi: 10.3390/su10020436

Houser, C., 2011. Sediment resuspension by vessel-generated waves along the Savannah River, Georgia. J. Waterw. Port Coas. Ocean Eng. 137(5), 246-257.

Lawson, S.E., Wiberg, P.L., McGlathery, K.J., Fugate, D.C., 2007. Wind-driven sediment suspension controls light availability in a shallow coastal lagoon. Estuar. Coas. 30 (1), 102-112.

Loosanoff, V.L., 1962. Effects of turbidity on some larval and adult bivalves. In: Proceedings of the Gulf and Caribbean Fisheries Institute, 14, 80-95.

Malej, M., Shi, F., Smith, J.M., 2019. Modeling ship-wake-induced sediment transport and morphological change – Sediment module in FUNWAVE-TVD. ERDC/CHL CHETN-VII-20. Vicksburg, MS: U.S. Army Engineer Research and Development Center. http://dx.doi.org/10.21079/11681/32911

McLoughlin, S.M., Wiberg, P.L., Safak, I., McGlathery, K.J., 2015. Rates and forcing of marsh edge erosion in a shallow coastal bay. Estua. Coas. 38, 620-638.

Mojfeld, H.O., Lavelle, J.W., 1988. Formulas for velocity, sediment concentration and suspended sediment flux for steady uni-directional pressure-driven flow. NOAA Technical Memorandum ERL PMEL-83, Pacific Marine Environmental Laboratory, Seattle, Washington, 26 p.

Montes, N., Swett, R., Sidman, C., Fik, T., 2016. Offshore recreational boating characterization in the Southeast US. University of Florida Sea Grant Program, TP 226, https://www.flseagrant.org/wp-content/uploads/Tp_226_web.pdf

National Oceanic and Atmospheric Administration (NOAA) National Estuarine Research Reserve System (NERRS) system-wide monitoring program. Data accessed from the NOAA NERRS Centralized Data Management Office website: http://www.nerrsdata.org/ ; accessed on August 1st, 2019.

Nielsen, P., 1992. Coastal bottom boundary layers and sediment transport. In Advanced Series on Ocean Engineering; World Scientific: Singapore, p. 324.

Nortek, 2018. Nortek Manuals: the comprehensive manual for velocimeters, Nortek AS, p. 119.

Osborne, P.D., Boak, E.H., 1999. Sediment suspension and morphological response under vessel-generated wave groups: Torpedo Bay, Auckland, New Zealand. J. Coas. Res. 15(2), 388-398.

Ozturk, M., Work, P.A., 2016. Acoustic Doppler velocimeter backscatter for quantification of suspended sediment concentration in South San Francisco Bay. In: Proceedings of the 35th Int. Conf. Coas. Eng. ICCE'16, 12 p.

Parnell, K.E., McDonald, S.C., Burke, A.E., 2007. Shoreline effects of vessel wakes, Marlborough Sounds, New Zealand. J. Coas. Res. SI 50, 502-506.

Price, F.D., 2005. Quantification, analysis, and management of Intracoastal Waterway channel margin erosion in the Guana Tolomato Matanzas National Estuarine Research Reserve, Florida. Master's Thesis, Florida State University, Tallahassee, FL, USA.

Rouse, H., 1937. Modern conceptions of the mechanics of fluid turbulence. Trans. A.S.C.E. 102, 463-543.

Rouse, H., 1961. Fluid Mechanics for Hydraulic Engineers, Dover, New York, 422 p.

Safak, I., Angelini, C., Norby, P.L., Dix, N., Rodenberry, A., Herbert, D., Astrom, E., Sheremet, A., 2020a. Wave transmission through living shoreline breakwalls. Cont. Shelf Res. 211, 104268. https://doi.org/10.1016/j.csr.2020.104268

Safak, I., Norby, P.L., Dix, N., Grizzle, R., Southwell, M., Veenstra, J.J., Acevedo, A., Cooper-Kolb, T., Massey, L., Sheremet, A., Angelini, C., 2020b. Coupling breakwalls with oyster restoration structures enhances living shoreline performance along energetic shorelines. Ecolog. Eng. 158, 106071. https://doi.org/10.1016/j.ecoleng.2020.106071

Schwimmer, R.A., 2001. Rates and processes of marsh shoreline erosion in Rehoboth Bay, Delaware, USA. J. Coas. Res. 17(3), 672–683.

Sheremet, A., Gravois, U., Tian, M., 2013. Boat wake statistics at Jensen Beach, Florida. J. Waterw. Port Coas. Ocean Eng. 139, 286-294.

Silliman, B.R., He, Q., Angelini, C., Smith, C.S., Kirwan, M.L., Daleo, P., Renzi, J.J., Butler, J., Ozborne, T.Z., Nifong, J.C., van de Koppel, J., 2019. Field experiments and meta-analysis reveal wetland vegetation as a crucial element in the coastal protection paradigm. Current Biology 29: 1800–1806.https://doi.org/10.1016/j.cub.2019.05.017

Styles, R., Hartman, M.A., 2019. Effect of tidal stage on sediment concentrations and turbulence by vessel wake in a coastal plain saltmarsh. J. Mar.Sci. Eng. 7, 192. doi:10.3390/jmse7060192

Styles, R., Glenn, S.M., 2002. Modeling bottom roughness in the presence of wave-generated ripples. J. Geophys. Res. 107, No. C8, 3110, 10.1029/2001JC000864

Tournadre, J., 2014. Anthropogenic pressure on the open ocean: the growth of ship traffic revealed by altimeter data analysis. Geophys. Res. Lett. 41, 7924-7932.

van Straaten, L.M.J.U., Kuenen, P.H., 1958. Tidal action as a cause of clay accumulation. J. Sedimen. Petrol. 28, 406-413.

Wiberg, P.L., Carr, J.A., Safak, I., Anutaliya, A., 2015. Quantifying the distribution and influence of non-uniform bed properties in shallow coastal bays. Limnol. Oceanogr. - Methods 13(12), 746–762. DOI: 10.1002/lom3.10063

Table 1: Volumes and rates of sediment transport

Days	Boat activity	Volume (m^3/m)	Rate ($m^3/m/hr$)
1-8	Yes	4.58	0.048
	No	4.27	0.043
9-11	Yes	3.70	0.085
	No	1.17	0.040
Total	Yes	8.28	0.059
	No	5.44	0.042

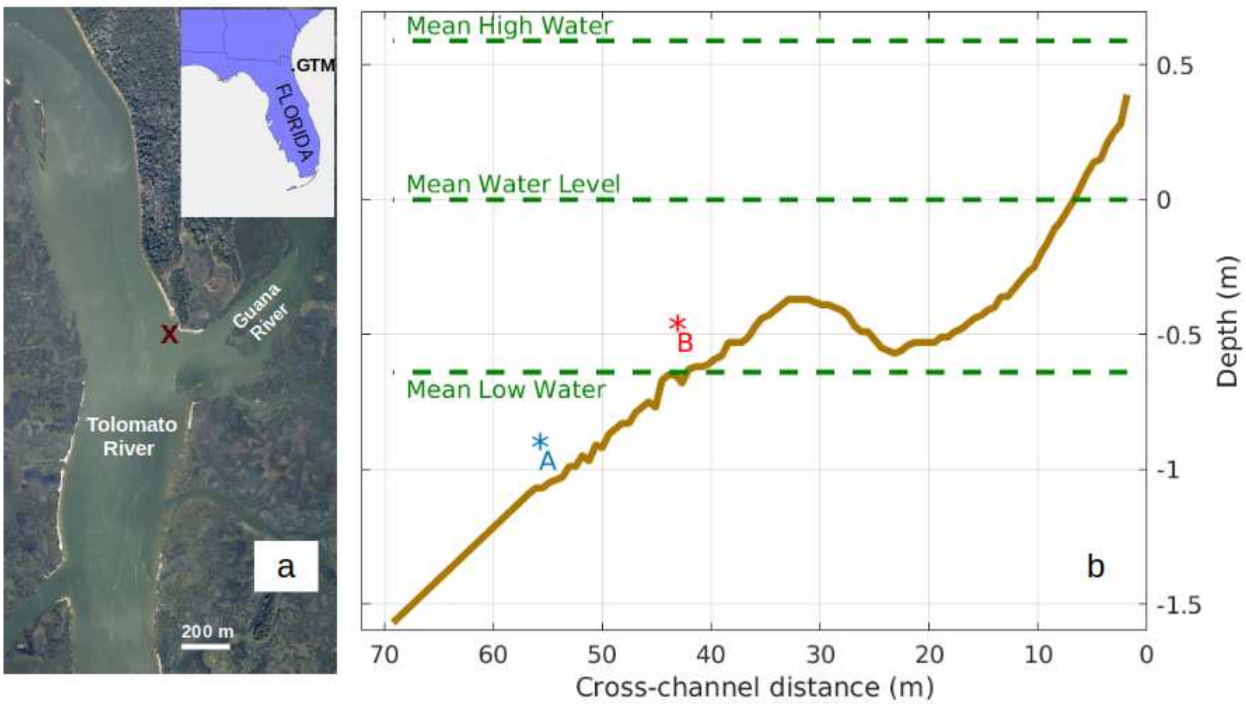

Figure 1: (a) The aerial view of the location of the cross-channel transect (marked with an ‘x’) of the instrumented platforms (A and B), and (b) the cross-channel bathymetry (dark brown). Inset panel at the top right of the aerial view shows where the site is located in Northeast Florida, USA; the aerial view shows the location of the experiment (29.986391° Latitude North, 81.327358° Longitude West) along the Tolomato River within the Atlantic Intracoastal Waterway. The river channel is about 400 m wide at the location of the transect. In the bathymetry figure in panel (b), mean high, mean and mean low water levels during the experiment are indicated with dashed green lines; vertical scale is exaggerated for clarity. The aerial view is obtained from the United States Geological Survey EarthExplorer database.

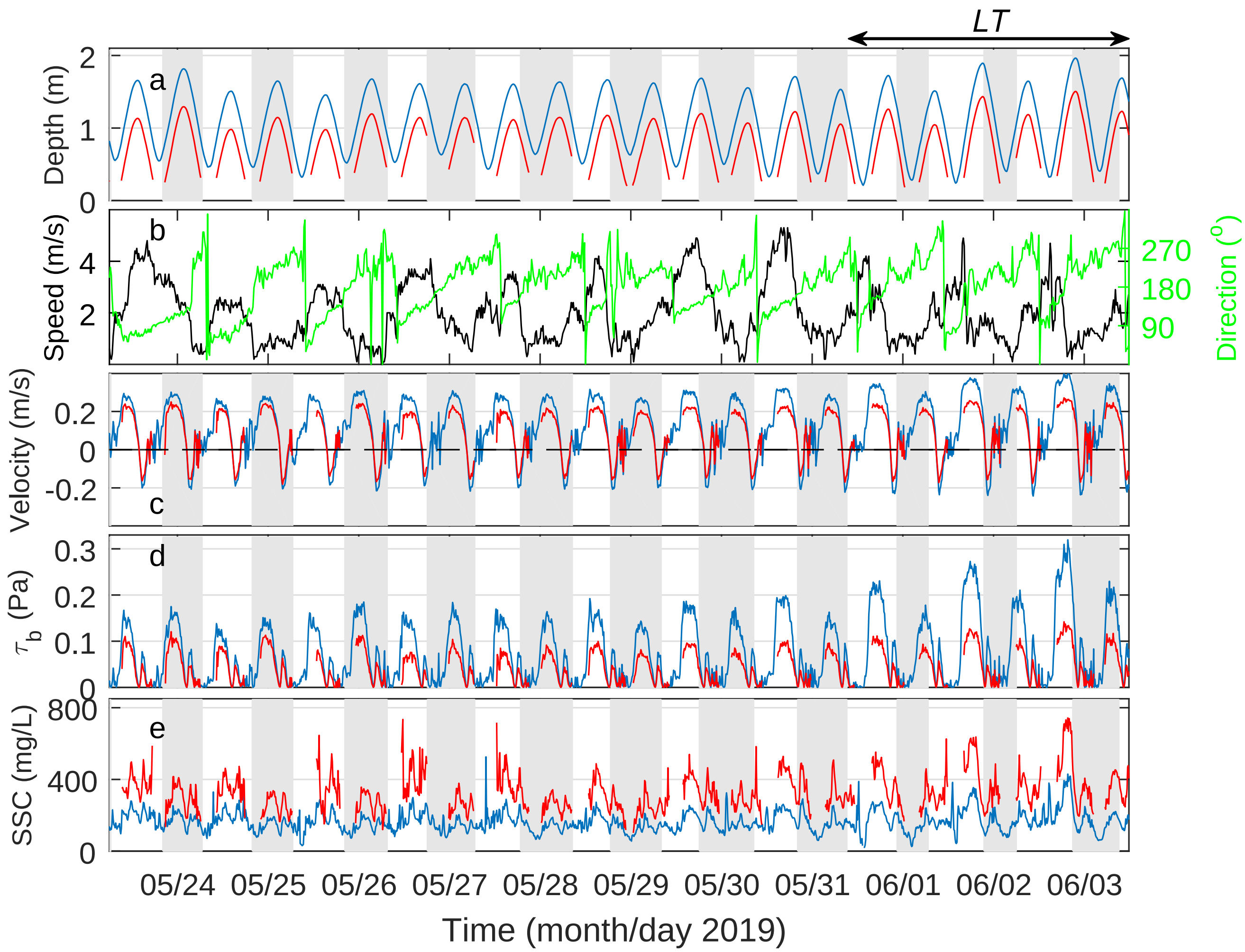

Figure 2: Time evolution of general conditions throughout the experiment: (a) water depth at Station A (blue) and Station B (red), (b) wind speed and direction, (c) current velocity at 0.17 meters above bed (mab) at Station A and Station B (positive and negative velocities indicate ~northward and ~southward flows, respectively), (d) shear stress at bed, and (e) suspended sediment concentration at 0.17 mab at Station A and Station B. The values are 10-min averages. The gaps in the data from Station B correspond to the low-tide periods when the data quality was low at very shallow water or the sensor volume at that point was out of the water. The grey shaded areas indicate the night periods of boat inactivity. The 'LT' annotation at the top panel indicates the spring tide period with relatively large tidal fluctuations and current speeds in the last part of the experiment.

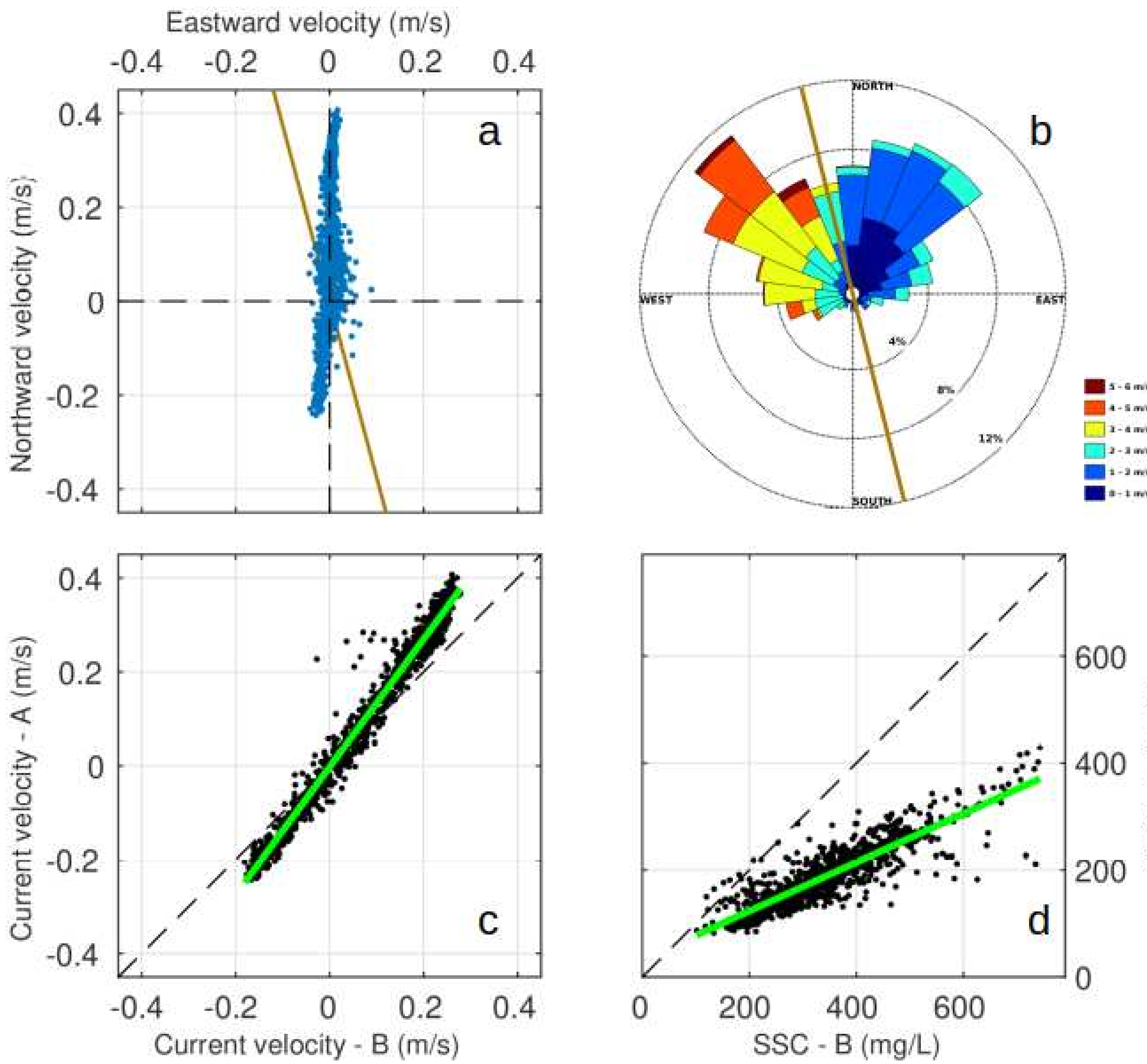

Figure 3: (a) Variation of northward current velocities with eastward current velocities at Station A, (b) wind rose during the experiment, (c) variation of current velocities at Station A with those at Station B, and (d) variation of suspended sediment concentrations at Station A with those at Station B. The current velocities and suspended sediment concentrations are 10-min averages. The wind rose in panel (b) shows where the winds were blowing to. The thick brown lines in panels (a) and (b) indicate the approximate orientation of the shoreline onshore of the transect. The thick green lines in panels (c) and (d) indicate the linear least square regressions (with r^2 of 0.97 and 0.79, respectively). The dashed black lines in panels (c) and (d) indicate the one-to-one relationships.

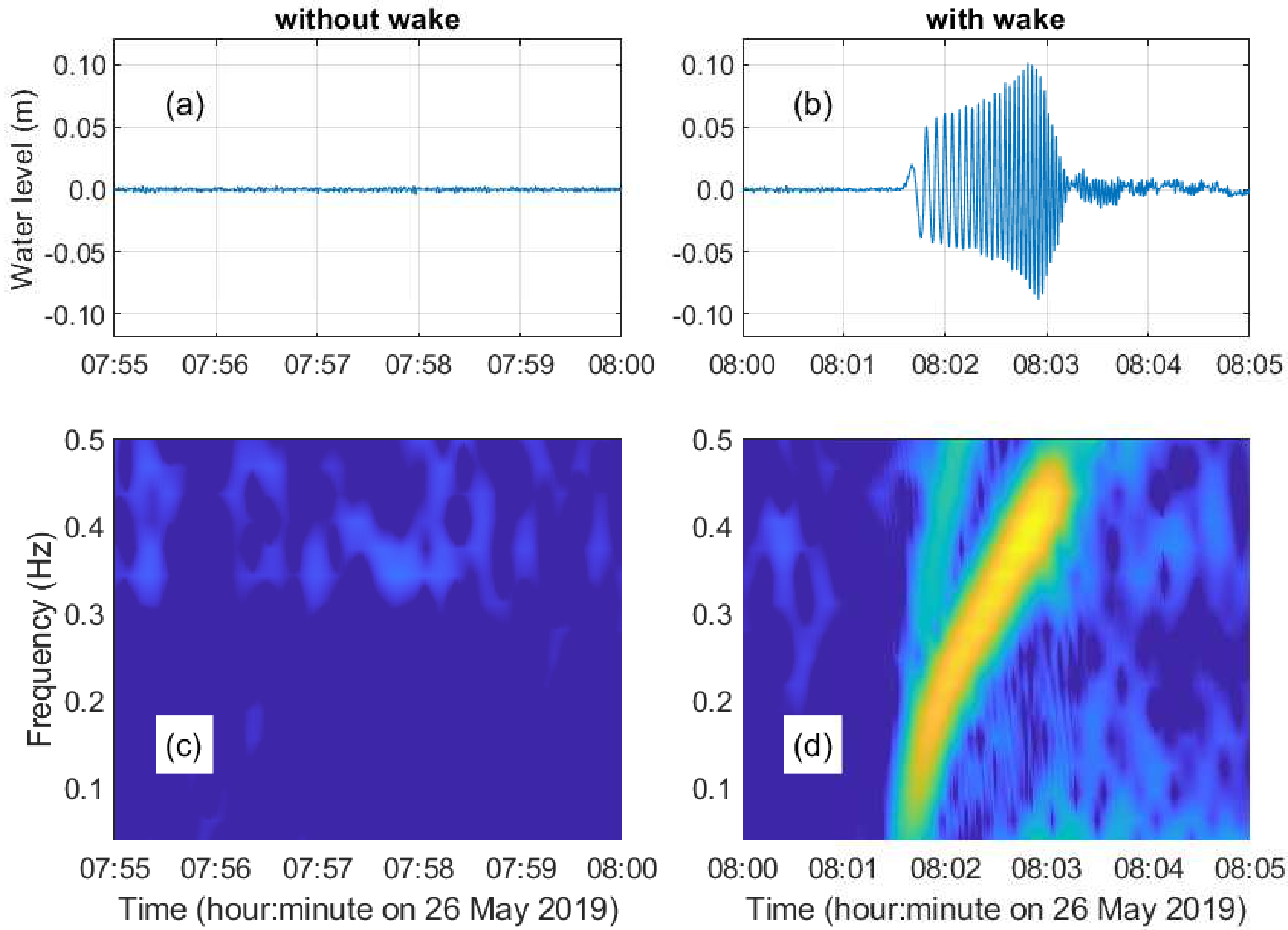

Figure 4: De-tided water levels (a-b) and normalized spectrograms (c-d) of two five-minute-long segments measured at Station A on 26 May 2019. Warm colors in (c-d) indicate high energy. The panels on the left and the right sides correspond to conditions without wakes and with wakes, respectively.

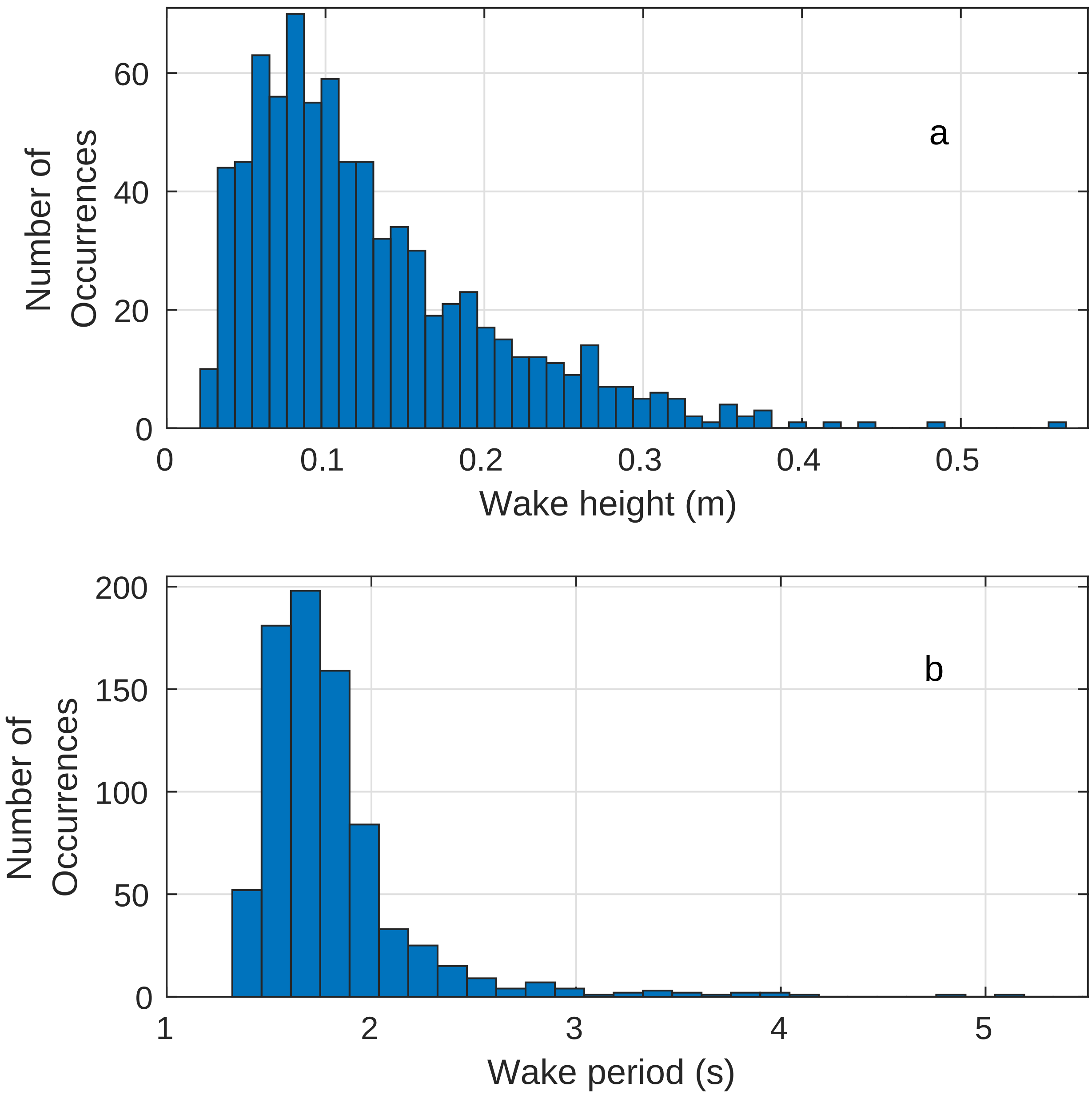

Figure 5: Histograms of (a) wake height, and (b) wake period at Station A.

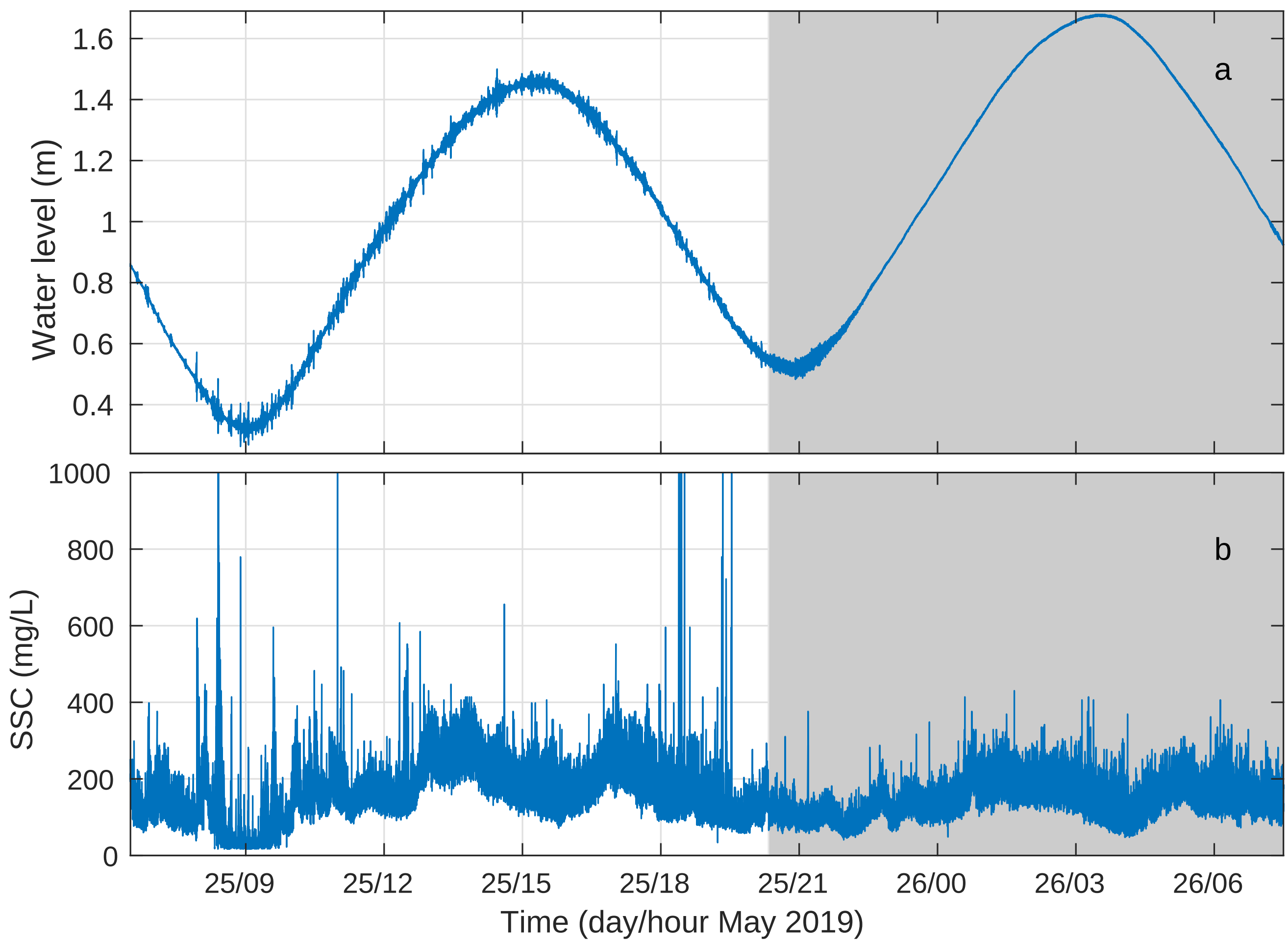

Figure 6: Time evolution of: (a) water level, and (b) suspended sediment concentration at 0.17 mab at Station A between 25 May and 26 May. The values are 8-Hz raw data. The areas shaded in gray indicate the night time of boat inactivity with no wakes.

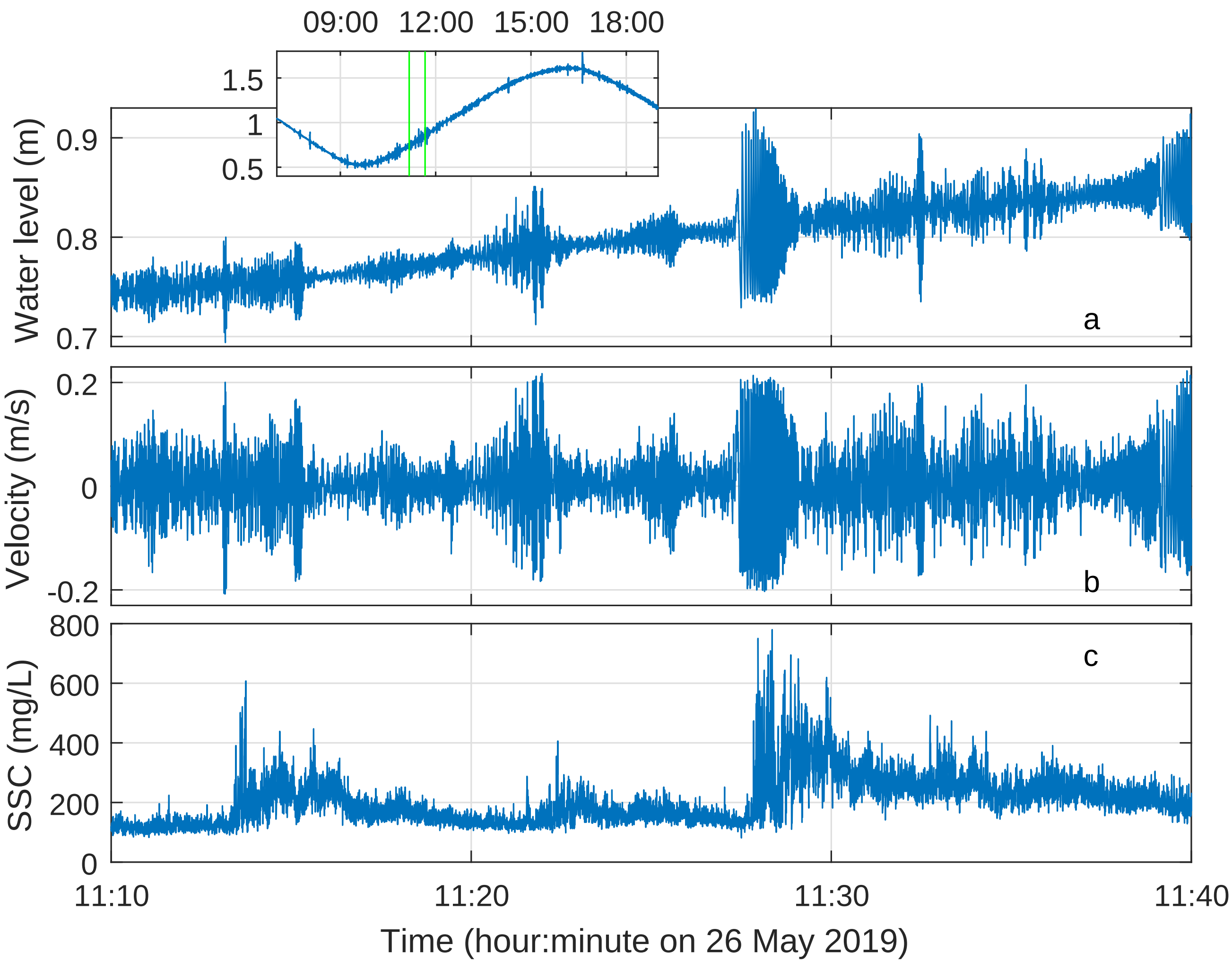

Figure 7: Time evolution of: (a) water level, (b) flow velocity, and (c) suspended sediment concentration at 0.17 m above bed at Station A during the wake events between 11:10 and 11:40 on 26 May 2019. The values are 8-Hz raw data. The green lines in the inset indicate the tidal phase that corresponds to the 30-min-long time-series in panels (a), (b), and (c).

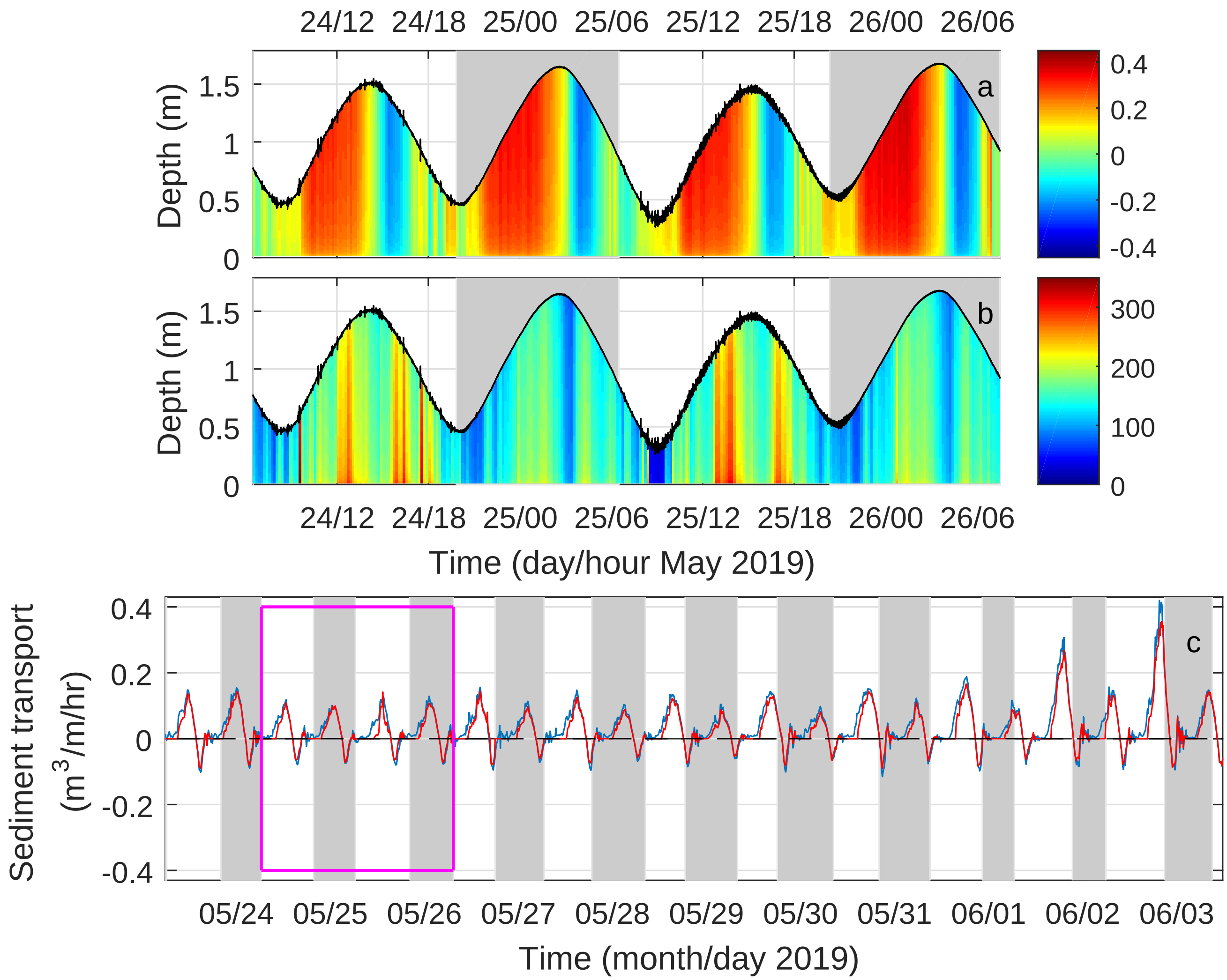

Figure 8: Time evolution of: (a) vertical structure of current velocity (m/s; positive and negative indicate ~northward and ~southward flow, respectively) at Station A between May 24th and 26th, (b) vertical structure of SSC (mg/L) at Station A between May 24th and 26th, and (c) depth-integrated horizontal sediment volume flux per unit width at Station A (blue) and Station B (red) throughout the experiment. The grey shaded areas indicate the night periods with no boat activity. The wake events are visible in the 8-Hz data (in black) inserted on the vertical structures of mean currents and SSC. The magenta rectangle in panel (c) indicates the time period for which the data of panels (a) and (b) are shown.

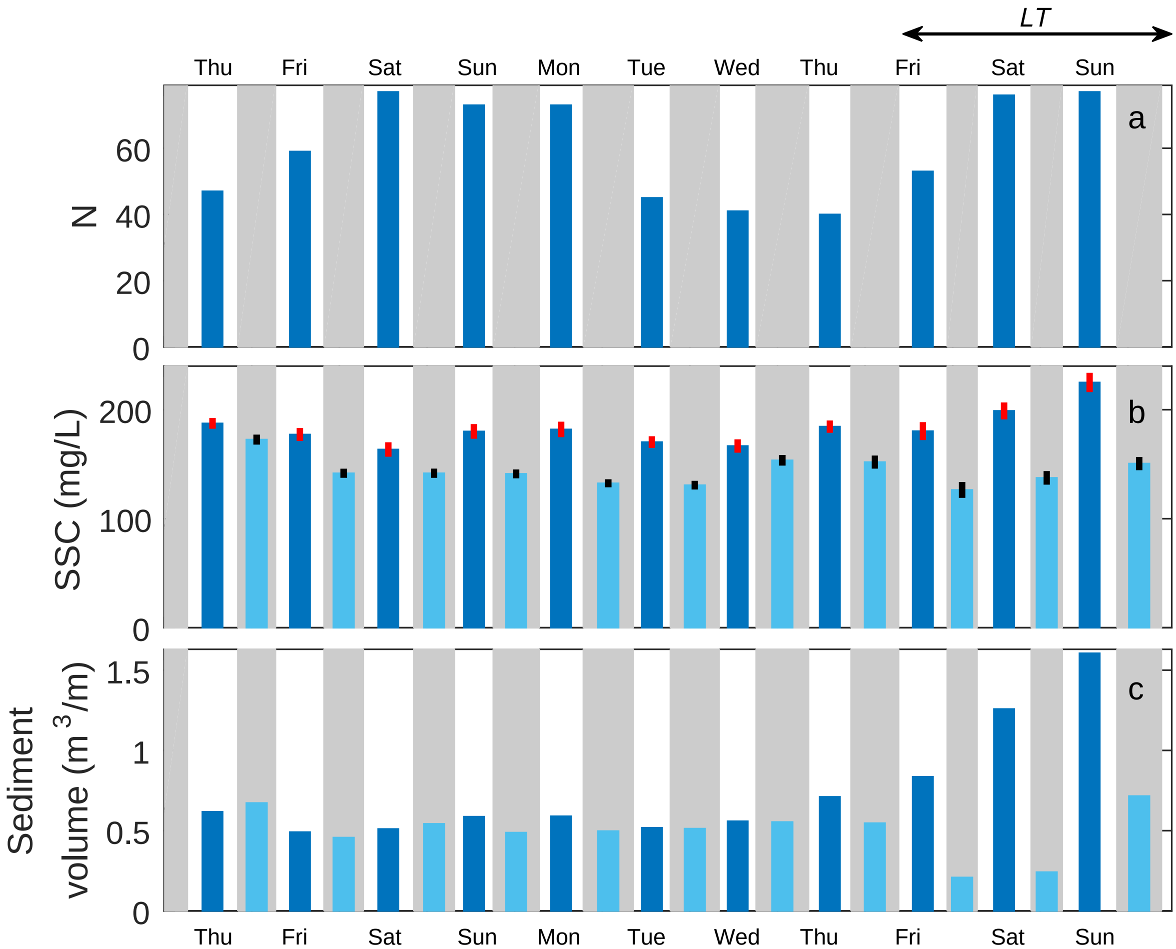

Figure 9: Variation of (a) total number of wake events during each boat activity period, (b) boat activity (dark blue) and boat inactivity period (light blue) averages of suspended sediment concentration at 0.17 mab, and (c) total sediment volume transported during boat activity (dark blue) and boat inactivity periods (light blue). Grey shaded areas highlight the boat inactivity periods. Vertical red and black bars in panel (b) show ± standard error during boat activity and boat inactivity periods, respectively. The annotation at the top panel indicates the period with relatively large tidal fluctuations and current speeds in the last part of the experiment (Figure 2).

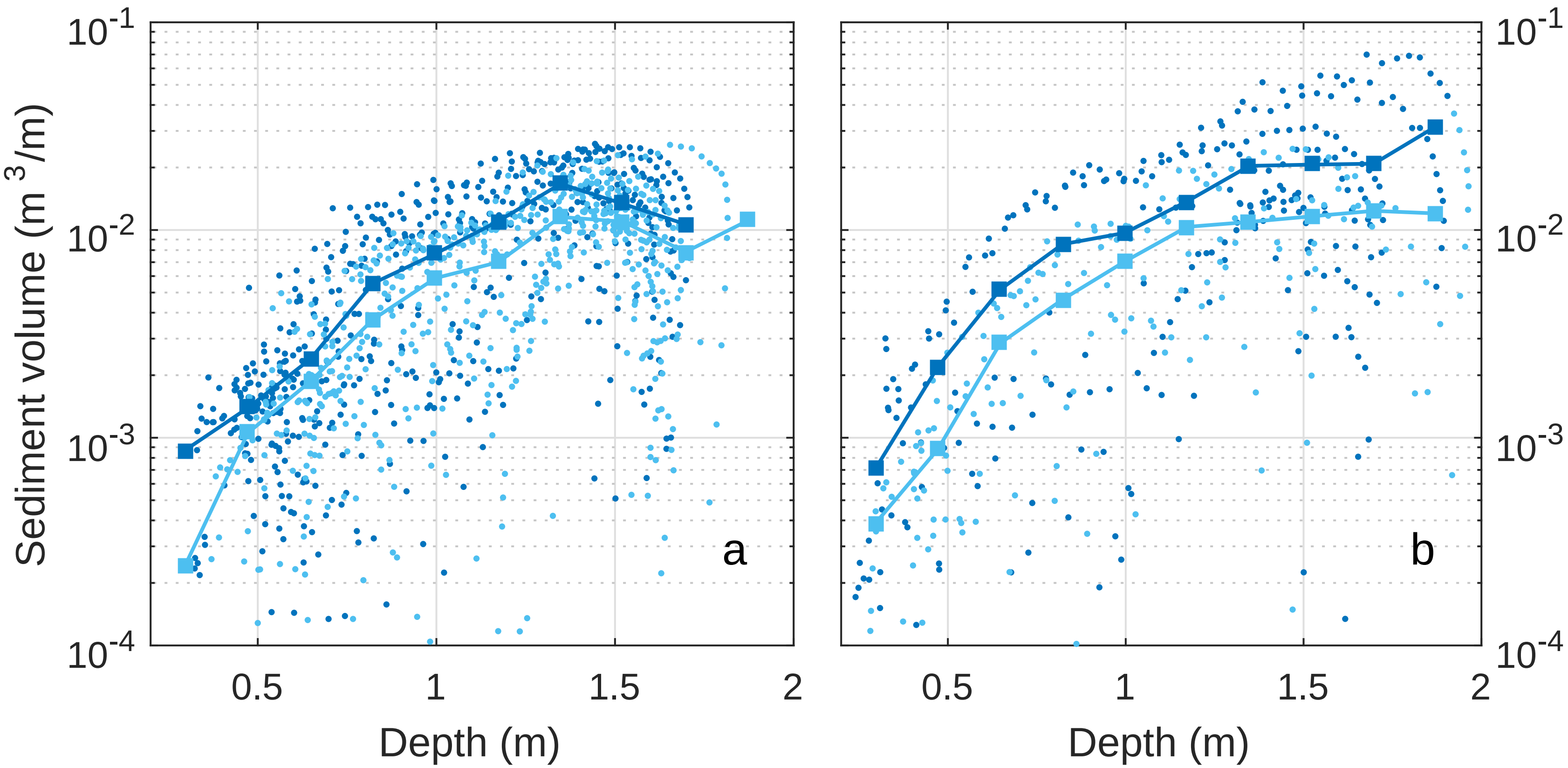

Figure 10: Volume of sediment transported at Station A during boat activity (dark blue) and inactivity (light blue), as a function of water depth. The two panels correspond to the results for (a) the first eight days, and (b) the last three days of the experiment. Dots show the volume estimates representing the 10-min intervals; the squares are averages over 18-cm-wide depth bins.